RSC Advances

PAPER

View Article Online
View Journal | View Issue

Cite this: *RSC Adv.*, 2024, **14**, 33068

Synthesis, characterization and application of silk sericin-based silver nanocomposites for antibacterial and food coating solutions

Shubhajit Shaw,[a] Rittick Mondal,[a] Paulami Dam,[a] Avijit Mandal,[b] Ritwik Acharya,[a] Sanjeet Manna,[c] Debnirmalya Gangopadhyay*[a] and Amit Kumar Mandal*[a]

Received 1st October 2024
Accepted 15th October 2024

DOI: 10.1039/d4ra07056a

rsc.li/rsc-advances

The rising demand for fresh and safe food is driving advancements in preservation technologies, with nanoparticles offering a revolutionary solution. These particles extend shelf life, preserve nutritional value, and enhance food safety, aligning with present consumer expectations. This study explores the eco-friendly synthesis, characterization, and application of silk sericin-based silver nanoparticles (SS-AgNPs) for antibacterial and food coating purposes. Silk sericin, a byproduct of the silk industry, is typically discarded despite its valuable properties like biocompatibility, biodegradability, and antimicrobial activity. In this research, sericin from *Bombyx mori* cocoons was used as a reducing and stabilizing agent to synthesize SS-AgNPs. Characterization was performed using UV-vis spectroscopy, Fourier-transform infrared spectroscopy (FTIR), X-ray diffraction (XRD), scanning electron microscopy (SEM), and dynamic light scattering (DLS). Antibacterial tests confirmed the efficacy of SS-AgNPs against *Pseudomonas* sp. and *Staphylococcus* sp., while food coating trials on tomatoes significantly reduced weight loss and microbial contamination. Biocompatibility was further verified through hemolysis and MTT assays, confirming SS-AgNPs' safety for biomedical and food-related uses. This study underscores the potential to convert sericin waste into a valuable resource, promoting sustainability and increasing the commercial value of sericulture.

1. Introduction

Silk sericin, a natural protein produced by the silkworm *Bombyx mori*, is an essential component for the formation of silk filament. This protein coats the fibroin filament, providing essential protection and adhesion during the silk-spinning process. Traditionally, sericin has been viewed as a waste product in the silk industry, despite its inherent beneficial properties.[1,2] It is estimated that the yearly worldwide production of dry cocoons, approximately 4 lakh MT, generates around 0.5 lakh MT of sericin waste, which poses significant disposal challenges.[3] This environmental issue has spurred growing interest among researchers to explore the potential applications of sericin. Recent studies have highlighted valuable properties of sericin, including its biocompatibility, biodegradability, and diverse biological activities including antibacterial, antioxidant, and anti-inflammatory properties.[1,3–5] These attributes are transforming sericin from a mere byproduct into a valuable resource with a wide range of innovative applications.

The antioxidant and antimicrobial properties of sericin make it particularly beneficial in health and cosmetic industries.[1,3] Its biocompatibility and biodegradability further enhance its potential for medical and pharmaceutical uses, while its moisturizing properties and UV resistance make it a preferred ingredient in skincare products[6] Sericin also demonstrates considerable thermostability, which is notably influenced by the method of extraction. Studies revealed that sericin exhibits an endothermic degradation peak around 220 °C when subjected to extraction under conditions of elevated temperature and pressure, surpassing the 210 °C observed with alternative extraction techniques.[7] Besides, application of sericin in food packaging can extend shelf life, and its consumption may improve the bioavailability of essential minerals like Zn and Fe.[8,9] These qualities underscore the growing research interest in leveraging potential of sericin across various fields.

Of late, incorporation of sericin into nano-conjugates has emerged as a promising area of research. Silk sericin-based nano-conjugates (SS-conjugates) impact the unique properties of sericin to enhance the efficacy and stability of nanomaterials. Perusal of literature reveals various studies exploring the use of sericin in developing drug delivery systems, tissue engineering scaffolds, and antimicrobial agents. These studies highlight versatility of sericin in creating functional nano-conjugates to

[a]*Department of Sericulture, Raiganj University, Raiganj 733134, West Bengal, India. E-mail: debn4u@gmail.com; amitmandal08@gmail.com*

[b]*Department of Life Sciences, Presidency University, Kolkata, 700073, India*

[c]*Central Instrumentation Facility, Odisha University of Agriculture and Technology, Bhubaneswar, 751003, Odisha, India*

address specific challenges in biomedical and industrial applications because of its large surface area relative to its volume. For instance, Dan *et al.*[10] demonstrated the potential of sericin-based nanoparticles for targeted drug delivery, while exploring sericin-based nanocarriers for controlled release of therapeutic agents. Das *et al.*[2] reviewed sericin-based scaffolds for tissue engineering, emphasizing their applications and properties. Additionally, recent findings shows effectiveness of sericin in antimicrobial applications through its conjugation with silver nanoparticles (AgNPs).[3,11,12]

Silver nanoparticles (AgNPs) are extensively utilized across various industries because of their distinctive properties, particularly their antimicrobial activity and cost efficiency.[13] In the commercial sector, AgNPs are employed in textiles, medical devices, and food packaging due to their ability to inhibit bacterial growth and extend product shelf life.[14,15] Recently, application of AgNPs in food coatings represents a promising approach to enhance food safety and quality. It is now possible to create barriers by incorporating AgNPs into food packaging to reduce microbial contamination, thereby extending the shelf-life of food products and reducing spoilage.[16] However, the use of AgNPs, in food coatings, from a safety perspective, must be carefully regulated to ensure they do not pose toxicity risks. The U.S. Environmental Protection Agency (EPA) has established particular thresholds for the concentration of silver nanoparticles in consumer products to ensure safety. For instance, the EPA tolerates silver levels in food contact materials up to 0.01% (10 000 ppm).[17] Adhering to these limits ensures that AgNPs can be utilized safely in food packaging applications without adverse health effects.

In this study, AgNPs were synthesized adopting a simple, efficient, and environmentally friendly method utilizing silk sericin. The research focuses on characterizing and assessing the practical significance of these silk sericin-based silver nanocomposites (SS-AgNPs), with the goal of converting waste sericin into a valuable product. Silk sericin, extracted from *B. mori* silk cocoons, was utilized as a reducing and stabilizing agent. The synthesized SS-AgNPs were characterized using various bio-physical techniques. Moreover, the biocompatibility and antibacterial activity of these SS-AgNPs were assessed against mostly commonly food-rotting bacteria such as *Pseudomonas* sp., and *Staphylococcus* sp. Further, the possibility of exploration of SS-AgNPs solution as effective food coating material was also evaluated. The study not only helps in making practical use of sericin waste but also enhances the commercial value of silk products, contributing to a more sustainable sericulture industry.

2. Experiment design

2.1. Collection, isolation and extraction of silk sericin

Silk cocoons of the multivoltine mulberry silkworm breed, Nistari were collected from the Silkworm Breeding Laboratory of the Department of Sericulture at Raiganj University, West Bengal, India. The hot water extraction method was employed following the method of Nam *et al.*[18] with slight modification. The cocoons were first chopped into small pieces and then 10 g of such cut cocoons were placed into a 500 mL Erlenmeyer flask containing 250 mL of deionized water and 0.2% sodium carbonate (Na_2CO_3). The extraction process was carried out in an autoclave at 121 °C for 30 min. Then, the mixture was passed through Whatman filter paper (no. 1) and dried for 24 h at 60 °C into a powder form for further experiments.

2.2. Preparation of sample

Firstly, 80 mL of $AgNO_3$ (10 mM) solution was transferred to a 250 mL Erlenmeyer flask and placed on a magnetic stirrer. Subsequently, 10 mL of a 1% (w/v) sericin solution (pH 11) was added to the stirred $AgNO_3$ solution.[19] The impact of Ag^+ ion concentration on AgNPs production was investigated by adjusting the different concentrations of $AgNO_3$ to 1–10 mM. Based on a previous study,[20] the 1 mM $AgNO_3$ solution was selected for future experiments due to its superior stability and uniformity. The observed yellow-brown colour change in the $AgNO_3$ solutions upon adding SS indicated the reduction of Ag^+ to Ag^0. The solutions were then mixed at 250 rpm and kept overnight at ambient temperature. The resulting SS-AgNPs were purified *via* centrifugation, dried at 50 °C and stored at 4 °C for further analysis.[19,21,22] The detailed step-by-step process of synthesizing SS-AgNPs is presented in Scheme 1.

2.3. Characterization of silk sericin-based silver nano composites (SS-AgNPs)

2.3.1. UV-vis spectroscopy. The preliminary characterization of SS-AgNPs was carried out using UV-vis spectroscopy to observe the conversion of Ag^+ ions into metallic Ag^0. Absorption spectra for both the SS extract and the synthesized SS-AgNPs were obtained with a UV-vis spectrophotometer. (Labman, LMSP-UV1900) over the wavelength range of 300 to 700 nm.

2.3.2. Fourier-transform infrared spectroscopy (FT-IR) analysis. The FT-IR spectra of the prepared SS extract and synthesized SS-AgNPs were analyzed using PerkinElmer (Spectrum Two, part no. L1600235) to investigate the functional groups of SS which was responsible for the formation and stabilization of the SS-AgNPs.

2.3.3. X-ray diffraction (XRD) analysis. The XRD pattern was obtained using a Rigaku Miniflex X-ray diffractometer, scanning the 2θ range of 20°–80° at 40 keV. The X'pertHighscore

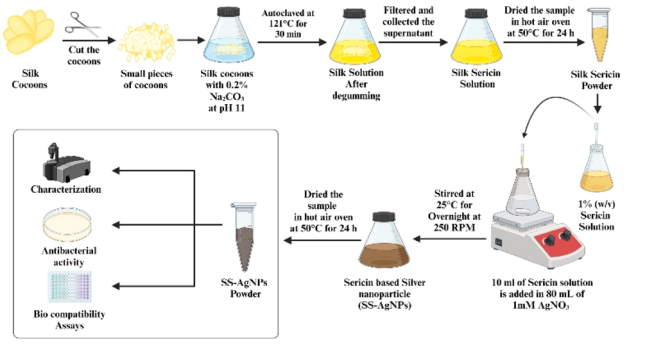

Scheme 1 Schematic diagram of detailed step-by-step process of synthesizing SS-AgNPs.

Plus software processed the data, identifying and fitting the diffraction peaks. The particle size D was determined using Scherrer's equation.[23]

$$D = (0.9 \times \lambda)/(\beta \operatorname{Cos} \theta)$$

where, K represents the Scherrer constant (usually 0.9), λ denotes the X-ray wavelength (1.5406 Å for CuK_{α}), β is the full width at half maximum (FWHM) of the peak in radians, and θ is the Bragg angle.

2.3.4. Scanning electron microscope with energy-dispersive X-ray spectroscopy (SEM-EDS) analysis. The surface morphology of biosynthesized SS-AgNPs was analyzed using a scanning electron microscope (SEM-EDX; S4160 Hitachi, Japan) following a standard procedure for sputter coating and imaging.[24] Prior to imaging, the samples were prepared by coating them with a thin layer of gold to enhance conductivity and prevent charging under the electron beam. This was achieved using the direct current sputter coating technique (Emitechk450X, England), where the sample was placed in a vacuum chamber, and a gold target was bombarded with ions. The resulting gold atoms were deposited onto the sample, creating a uniform, conductive layer. Once coated, the samples were placed in the SEM chamber for analysis, allowing for high-resolution imaging of the surface morphology and elemental composition verification *via* energy-dispersive X-ray spectroscopy (EDX). This process ensured clear, detailed images with minimal distortion or artifacts.

2.3.5. Dynamic light scattering (DLS) analysis. DLS was performed using a Litesizer DLS 500 (83382307, Anton Parr, AUSTRIA) to determine the zeta potential of the synthesized SS-AgNPs.[25] The sample was diluted with deionized water, and measured at 25 °C to assess surface charge and stability of the SS-AgNPs nanocomposites.

2.4. Antimicrobial potential of SS-AgNPs

2.4.1. Isolation and enumeration of bacteria from tomatoes. On the 18th day, when the tomatoes in the uncoated (control) group had fully rotted, samples from all the SS-AgNPs-coated, agar-coated and uncoated groups were collected using sterile cotton swabs to assess total viable counts of culturable bacteria. The swabs were then placed in PBS (1X) solution and spread on nutrient agar medium plates, and incubated overnight at 37 °C.[26] Furthermore, individual colonies were selected after incubation and moved to a fresh medium to achieve pure colonies. The isolates were stored at −70 °C in 20% glycerol for future use.

2.4.2. Molecular identification of tomato spoiling bacteria. The genomic DNA of the four isolates (*i.e.* RTCS1, RTCS2, RTTS1, RTTS2) were extracted using the phenol:chloroform method, as described earlier.[27] The 16S rDNA was amplified using universal primers 27F, 704F, and 907R.[28] Purified 16S rDNA was sequenced using the Sanger sequencing method. Both strands of sequenced nucleotides were aligned through BioEdit software (**http://www.bioedit.software.informer.com**) to retrieve the partial/complete sequence of the 16S rDNA of the isolate. The retrieved 16S rDNA sequence was submitted to the EZBioCloud server (**https://www.ezbiocloud.net/**) to identify the closest type strains. From the EZBioCloud server, all the closest type strains for the isolated strains were downloaded to obtain multiple sequence alignment with the ClustalW program using MEGA11 software. Phylogenetic trees were constructed by the neighbor-joining (NJ) method, where the evolutionary distances were calculated by the Kimura 2 parameter model. Bootstrap analysis for the phylogenetic tree was executed with resampling 1000 times for the validation of each clade of the phylogenetic tree.[29] The NCBI accession number for the 16S rDNA sequence of RTCS1, RTCS2, RTTS1, RTTS2, were PQ211073, PQ268966, PQ268967, and PQ268969, respectively.

2.4.3. Assessing the antimicrobial activity of SS-AgNPs and sericin. Antimicrobial activity of SS-AgNPs and sericin was conducted *via* the agar well diffusion method to evaluate the effectiveness against the isolated tomato rotting bacteria from the uncoated tomatoes RTCS2 and RTTS2. Pure bacterial cultures were evenly spread on Mueller–Hinton agar (MHA) plates, and 8 mm diameter wells were created using a cork borer. A volume of 100 μL of the synthesized SS-AgNPs (1 mM) and a 1% (w/v) silk sericin solution were introduced into their respective wells and incubated overnight at 37 °C. The zones of inhibition were measured following incubation.

2.4.4. Measurement of minimum inhibitory concentration (MIC). The concentration of MIC of biosynthesized SS-AgNPs were conducted following the CLSI guidelines. The MIC test was carried out in a 96-well round-bottom microtiter plate using standard broth microdilution techniques. The bacterial inoculum was adjusted to a concentration of 10^6 CFU mL^{-1} 100 μL of the synthesized SS-AgNPs stock solution (1000 μg mL^{-1}) was added and sequentially diluted twofold with the bacterial inoculum in 100 μL of MHB from column 12 to column 3. Column 12 of the microtiter plate had the highest concentration of AgNPs, while column 3 had the lowest. Column 1 acted as a negative control (medium only) and column 2 served as a positive control (medium plus bacterial inoculum).

2.5. Biocompatibility of SS-AgNPs

2.5.1. Cell line assay. An MTT (3-[4,5-dimethylthiazole-2-yl]−2,5-diphenyltetrazolium bromide) assay was conducted to assess the cytotoxicity of the synthesized SS-AgNPs.[22,29] The synthesized SS-AgNPs at various concentrations, such as 12.5 μg mL^{-1}, 25 μg mL^{-1} 50 μg mL^{-1}, 100 μg mL^{-1}, 200 μg mL^{-1}, and 400 μg mL^{-1} were treated with Hek293 (human embryonic kidney 293 cell line) (ATCC) cell lines (10^5 no. of cells) in a 96-well micro-plate, and incubated for 24 h at 37 °C in a 5% CO_2 incubator. After the incubation period, DMEM media (10% FBS) were replaced with 50 μL of MTT (1 mg mL^{-1} in 1X PBS) + 50 μL of DMEM media (FBS free), and incubated at 37 °C for 3 h. After that the previous media was discarded and 100 μL of DMSO, a formazan solubilizer was added to each well, and the plate was incubated for 35 min. The resulting color was measured by recording the absorbance at 570 nm in Biotek® Synergy H1 micro-plate reader (USA). The percentage cell cytotoxicity was calculated as follows-

$$\text{Cell cytotoxicity} = (A - B)/A \times 100$$

where, A represents the absorbance of control (untreated) cells and B denotes the absorbance of cells treated with different concentrations of synthesized SS-AgNPs.

2.5.2. Hemocompatibility study. The hemocompatibility study of SS-AgNPs was assessed using a hemolytic assay, following the study of Mondal *et al.*[29] The hemolytic assay study determined whether there were any adverse effects following the interaction between nanoparticles and blood cells. Diluted solution of bovine red blood cells (RBCs) was mixed with SS-AgNPs at a concentration of 50 μg mL^{-1}. The mixture was then incubated for 2 h at room temperature. After incubation, we separated the supernatant (liquid portion) from the RBCs. To measure hemolysis (RBC damage), UV-visible spectrophotometer (Labman, LMSP-UV1900) is used to assess the absorbance of the supernatant at 541 nm. The percentage of hemolysis was calculated using the following equation-

$$\text{Hemolysis (\%)} = [(A_s - A_N))/((A_P - A_N)] \times 100$$

where, A_S, A_N, A_P are the absorbance of the sample, negative control (1X PBS) and positive control (distilled water), respectively.

2.5.3. Toxicity assay on silkworm. The disease-free layings (dfls) of the mulberry silkworm, Nistari (pure multivoltine) were collected from the Office of the Assistant Director, Directorate of Textile Sericulture, Raiganj, Government of West Bengal. The rearing of the silkworm larvae was performed at silkworm rearing laboratory, Raiganj University during the month of June–July, 2024 adopting the standard protocols.[30] Silkworm larvae were fed with the mulberry leaves of S_{1635} grown at the departmental mulberry garden following the recommended agronomical package and practices as outlined by Dandin and Kumari.[31] Four batches were maintained including the control after 4th moult. Fifty silkworm larvae were kept in each batch for the study. The mulberry leaves were initially rinsed thoroughly with water and then air-dried. Three experimental batches such as T_1, T_2 and T_3 were fed with the mulberry leaves spread with synthesized SS-AgNPs at selected concentrations of 31.25 μg mL^{-1}, 62.5 μg mL^{-1} and 125 μg mL^{-1} respectively. The control batch was fed with mulberry leaves without any treatment. Three feedings were given per day and data were recorded for larval duration, larval survivability, larval weight and length, pupal survivability, silk gland weight, cocoon weight, cocoon shell weight, cocoon shell percentage, filament length, denier, fibroin and sericin content. Cocoon shell percentage, denier and sericin content were calculated using the following formulae-

$$\text{Cocoon shell \%} = (\text{coccon shell weight})/(\text{coccon weight}) \times 100$$

$$\text{Denier} = [\text{silk filament weight (g)})/(\text{silk filament length (m)}] \times 9000$$

$$\text{Sericin content \%} = (W_0 - W_1)/W_0 \times 100$$

where, W_0 (g) and W_1 (g) are the weights of the dried fiber before and after degumming with Na_2CO_3 solution, respectively.[32]

2.6. Evaluation of practical significance of SS-AgNPs

2.6.1. Preparation of SS-AgNPs based food coating material. SS-AgNPs were mixed with a 1% agar powder solution for the preparation of homogenized food coating material (see Scheme 2). The final concentration of AgNPs in the solution was maintained at 30 μg mL^{-1}.

2.6.2. Application of SS-AgNPs as food coating material. For the experiments, tomatoes were dip-coated once by immersing them in a 70 mm deep coating solution (30 μg mL^{-1} SS-AgNPs + 1% agar) at room temperature (25 ± 5 °C) for 2 min, removed by holding pedicel, and then air dried and marked as SS-AgNPs coated.[33] The tomatoes coated only with 1% agar solution without any AgNPs treatment were assigned as agar coated while, tomatoes without any coating kept as control group. A total number of 90 tomatoes (each group comprising 30) were used for this study. The tomatoes were kept in commercial crisper separately in groups and stored at 25 ± 5 °C and 65 ± 5 RH under normal environment until the samples started to get rotten.

2.6.3. Evaluation of SS-AgNPs as food coating material

2.6.3.1. Determination of weight loss percentage. The weight loss of the treated and control group tomatoes was monitored at room temperature, with observations recorded every 3 days up to the 18th day, when the control group tomatoes had fully decayed. The weight loss percentage was calculated using the following equation-

$$\text{Weight loss} = (M_N - M_0)/M_0 \times 100$$

where, M_N is the weight of the fruit on the day of sampling, and M_0 is the weight of the fruit on the 0th day.

2.6.3.2. Determination of decaying percentage. To determine the decay percentage of tomatoes, each sample from the SS-AgNPs-coated, agar-coated, and control groups were visually examined for the development of spots, followed by softening

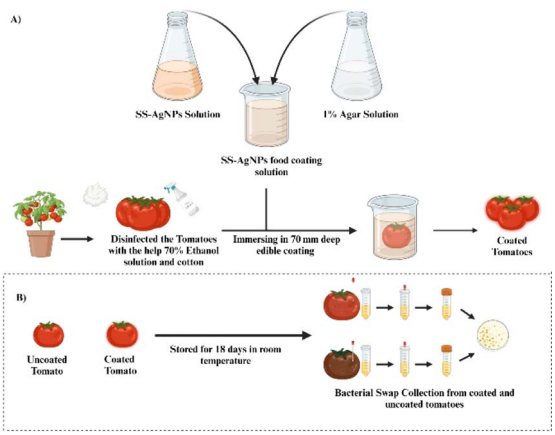

Scheme 2 Schematic representation of the (A) preparation of food coating material, (B) enumeration of the bacterial load from both coated and uncoated tomatoes.

and eventual deterioration. The number of rotting tomatoes in each group was counted, and the percentage of decayed tomatoes was calculated relative to the total number of tomatoes in each group.[34]

2.7. Statistical data analysis

All measurements were performed in triplicate to ensure accuracy and reproducibility. The mean values and standard deviations (SD) were computed for each set of measurements. Data were analyzed using one-way analysis of variance (ANOVA) to evaluate differences among the SS-AgNPs coated, agar coated and control groups following Dunnett's significant test analysis ($p < 0.05$). The statistical analysis was conducted using GraphPad Prism version 8.4.2., a software package designed for comprehensive data analysis and visualization.

3. Results and discussion

3.1. Characterization of SS-AgNPs

3.1.1. Ultraviolet-visible spectroscopy. The results on UV spectra of SS and SS-AgNPs are depicted in Fig. 1. The highest absorption peak of SS-AgNPs recorded at 428 nm (Fig. 1A). This peak may be due to the reduction of Ag^+ to Ag^0 by SS.[35] The inset of Fig. 1 (Fig. 1B) shows the color change in the aqueous SS solution from light yellow to dark brown indicating the formation of SS-AgNPs nanocomposites. One of the most fascinating properties of metal nanoparticles is their optical behavior, which varies with the shape and size of the nanoparticles.[36] Laser beams passing through the colloidal solution after the formation of SS-AgNPs display the Tyndall effect, where light scattering is observed (Fig. 1B). This light scattering pattern, indicative of the Tyndall effect, provides an initial indication of AgNPs formation in the solution. The Tyndall effect with AgNPs, which are microscopic colloidal particles sufficiently large to scatter a light beam, further confirms their presence.[25] The extent of light scattering is influenced by both the particle density in the colloidal structure and the wavelength of the incident light.[37]

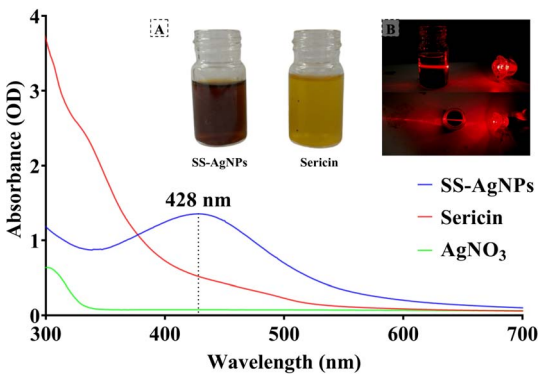

Fig. 1 UV-vis Spectra of SS-AgNPs, Sericin, and $AgNO_3$. (A) It corresponds to the solution of the 1 mM of SS-AgNP and silk sericin solution, (B) laser light scattering of SS-AgNPs solution in which the upper side of the figure corresponds side view and the lower side corresponds to the top view of light scattering.

3.1.2. Fourier-transform infrared (FT-IR) spectroscopy analysis. Results from the FT-IR analysis showed characteristic absorption peaks for SS and SS-AgNPs at 1641.1 cm^{-1} (amide-I), 1520 cm^{-1} (amide-II), and 1234.1 cm^{-1} (amide-III) for SS, and at 1637.6 cm^{-1} (amide-I), 1522.3 cm^{-1} (amide-II), and 1238 cm^{-1} (amide-III) for SS-AgNPs (Fig. 2). Comparable FT-IR patterns were reported during the production of SS-AgNPs, with absorption peaks at 1640 cm^{-1}, 1503 cm^{-1} and 1248 cm^{-1} for amide-I, II and III respectively.[38] Moreover, variations in band spectra were observed, with some bands shifting to slightly higher wavenumbers, such as from 1520 cm^{-1} to 1522.3 cm^{-1}, and from 1234.1 cm^{-1} to 1238 cm^{-1}. These shifts may result from the reduction of Ag ions, which can cause oxidation of certain functional groups.[38] The peak at 1637.6 cm^{-1} corresponds to carbonyl stretching frequency. The shift of the carboxylic group (COOH) stretching frequency from a higher wavenumber in SS to a lower wavenumber in SS-AgNPs might be due to Ag^+ reduction by the biomolecules in SS, which include COOH, OH, and CO groups that strongly adhere to the nanoparticle surface.[22] Additionally, the band at 3268.2 cm^{-1} in SS shifted to 3276.6 cm^{-1} in SS-AgNPs, indicating NH–OH bond stretching vibrations.[39] The small shift between 1392 to 1390 in SS-AgNPs to sericin which corresponds bending of –OH groups.[40] The shift from 1057.4 cm^{-1} in SS to 1063.6 cm^{-1} in SS-AgNPs suggested a strengthening of the C–O bond, likely due to the interaction between SS and SS-AgNPs, where SS acts as a stabilizing and capping agent.[41] The disappearance of the peak at 983 cm^{-1} in the SS-AgNPs FT-IR spectrum implies that the interaction with AgNPs had altered the chemical environment around the SS residues, causing a shift or masking of the C–O stretching vibration characteristic of SS.[42] Furthermore, a weak adsorption peak at 890 cm^{-1} corresponding to Ag–O indicated the incorporation of AgNPs with SS[35,43] (Table 1).

3.1.3. X-ray diffraction (XRD) analysis. The XRD patterns of the synthesized SS-AgNPs, as shown in Fig. 3, revealed their crystalline structure with distinct peaks at 32.4°, 38.4°, 46.5°, 64.8°, and 77.8°, corresponding to the (122), (111), (200), (220), and (311) planes of a face-centred cubic (FCC) structure of metallic silver (Ag), respectively. This confirms the FCC crystalline structure of the AgNPs, consistent with previous

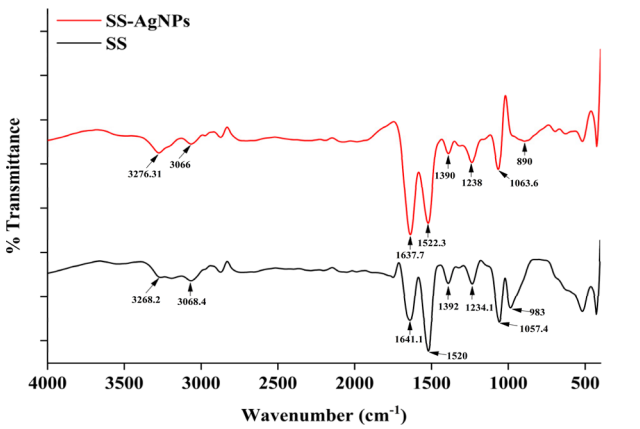

Fig. 2 FTIR-Spectra of SS-AgNPs and sericin.

Table 1 FTIR peaks of SS-AgNPs and sericin with band assignment

Peaks of SS	Peaks of SS-AgNP	Band assignment	Reference
3268.2	3276.6	NH–OH bond stretching	39
3068.4	3066	Aromatic C–H stretching band of tyrosine	41
1641.1	1637.6	Amide I (C=O stretching vibration)	19, 22 and 38
1520	1522.3	Amide II (N–H bending and C–N stretching vibration)	
1392	1390	Bending of O–H groups	40
1234.1	1238	Amide III (C–N–H in-plane bending and C–N stretching vibration)	19 and 38
1057.4	1063.6	C–O stretching	42
983	*x*	C–O stretching of serine	42
x	890	Ag–O	35 and 43

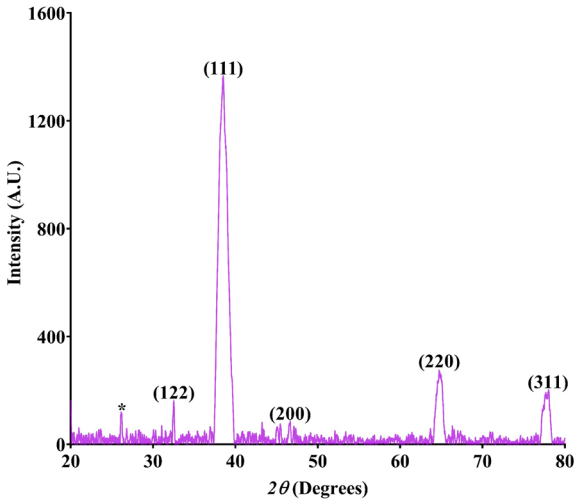

Fig. 3 X-ray diffraction pattern of the SS-AgNPs.

studies.[22,38,39,44–46] The most prominent peak appeared at a 2θ angle of 38.2°, which corresponded to the (111) plane, indicating that this plane was the dominant feature in the silver nanoparticles.[47] This suggests that the synthesized AgNPs exhibited a high degree of crystallinity. The peak at 26.15° is attributed to SS, indicating its incorporation into the AgNPs nanocomposites.[35] The average particle size of the SS-AgNPs ranged from 6–34 nm, with a crystallinity percentage of 76.19%, aligning with findings by Koley *et al.*[48] The full width at half maximum (FWHM) calculated from XRD data and characteristic patterns of the different crystalline structures of SS-AgNPs has summarized in Table 2. These results demonstrated the high quality and uniformity of the synthesized nanoparticles, confirming the effectiveness of the synthesis process. The observed structural features, including the presence of sericin, suggest potential applications in biomedical and material sciences due to the enhanced stability and biocompatibility of the SS-AgNPs nanocomposites.

3.1.4. Scanning electron microscopy (SEM). The SEM image of biosynthesized SS-AgNPs (Fig. 4) showed a polydispersed and irregular in form with no defined morphology. Factors like intermolecular attraction and hydrophobic interactions may have contributed to the collapsed structures observed.[49] Previous investigations by Khan *et al.*,[50] Riaz *et al.*,[51] and Labulo *et al.*[52] also reported similar findings, as they synthesized AgNPs using different natural sources. Khan *et al.*[50] utilized seed coat waste from pistachio (*Pistacia vera*), Riaz *et al.*[51] employed aqueous root extract of *A. glauca*, and Labulo

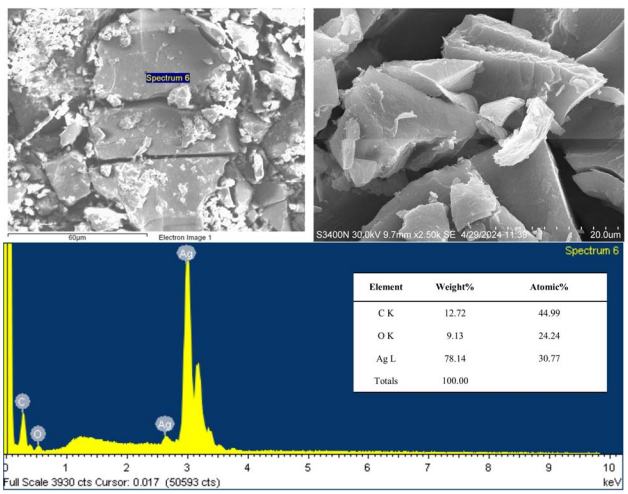

Fig. 4 SEM and EDX of the SS-AgNPs.

Table 2 X-ray diffraction scattering data of the SS-AgNPs

2θ	Plane	FWHM	Structure	Reference
26.15			Sericin	35
32.4	122	0.23889	Face-centered cubic crystalline structure of metallic AgNPs	46
38.4	111	1.27565		22, 38, 39, 44 and 45
46.5	200	0.25923		
64.8	220	0.82812		
77.8	311	0.85437		

et al.[52] used leaf extract from *Morinda lucida*. The EDX profile confirmed the presence of AgNPs through strong silver signals, while carbon peaks indicated the presence of carbon compounds, possibly from amino acids in the silk sericin extract, confirming the successful synthesis of AgNPs using SS extract.

3.1.5. Dynamic light scattering spectroscopy. The DLS analysis determined the zeta potential of bio-molecule-functionalized AgNPs in a colloidal aqueous solution (Fig. 5). The zeta potential of sericin-based AgNPs is a vital indicator of their stability and potential applications. Studies have shown that sericin effectively stabilizes AgNPs, with zeta potential values varying based on the synthesis method and conditions.[53] In this study, the SS-AgNPs revealed a zeta potential of approximately −43.86 mV, indicating significant stability and preventing nanoparticle aggregation through strong electrostatic repulsion.[49] To assess the tendency of AgNPs to aggregate and eventually precipitate, particle size distribution in the simple dispersion was used as a control parameter, alongside electro-kinetic or zeta-potential measurements. Typically, zeta-potential values exceeding ±25 mV are considered indicative of stable nano silver dispersion.[54,55]

3.2. Antimicrobial activities of SS-AgNPs

3.2.1. Enumeration of bacteria from tomatoes. The total bacterial count of the fruit samples was determined by assessing the bacterial colonies on each plate, corresponding to serial dilutions of 10^{-1}, 10^{-2}, and 10^{-3}, after which the mean value was calculated. TVC > 4 $\log_{10}$ CFU mL^{-1} is indicative of significant microbial presence and is directly associated with fruit spoilage.[56] Our study found that the mean TVC was 1.45 $\log_{10}$ CFU mL^{-1} for the SS-AgNPs coated sample, 6.60 $\log_{10}$ CFU mL^{-1} for agar coated sample and 9.54 $\log_{10}$ CFU mL^{-1} for the uncoated sample (control).

3.2.2. Molecular identification of bacteria from tomatoes. Four bacterial strains responsible for the spoilage of tomatoes have been identified. Two of these strains, *Pseudomonas* sp. RTCS2 and *Staphylococcus* sp. RTTS2 were obtained from uncoated tomatoes (control group). The remaining two strains, *Enterobacter* sp. RTCS1 and *Enterococcus* sp. RTTS1 were isolated from tomatoes coated with agar.

The 16S rDNA-based phylogenetic analysis of closely related type strains indicated that the closest relative to the isolates RTCS2 and RTTS2 were *Pseudomonas asiatica* RYU5 with 99.93% similarity (1 nt variation), and *Staphylococcus gallinarum* ATCC 35539 with 99.93% similarity (1 nt variation), respectively (Fig. 6).

Additionally, the EZBiocloud server identified *Enterobacter cloacae* subsp. dissolvens LMG 2683 as the closest relative to the isolate RTCS1, with a 99.79% similarity (3 nt variation). However, phylogenetic tree analysis indicated that RTCS1 was more closely related to *Enterobacter cloacae* subsp. cloacae ATCC 1304, with a 99.73% similarity (4 nt variation). These findings suggest that RTCS1 may represent a novel species, warranting further genomic analysis for confirmation. Moreover, it was also observed that the closest relative to the isolate RTTS1 was the *Enterococcus casseliflavus* MUTK 20 and *Enterococcus innesii* GAL7 with 100% similarity (0 nt variation) (Fig. 7).

3.2.3. Zone of inhibition test. The synthesized SS-AgNPs demonstrated significant antibacterial activity, with inhibition zones of 20 ± 0.5 mm against *Pseudomonas* sp. RTCS 2 (Fig. 8A) and 16 ± 0.4 mm against *Staphylococcus* sp. RTTS2 (Fig. 8B). In comparison, the silk sericin exhibited much lower antibacterial activity, showing inhibition zones of 2 ± 0.2 mm for *Pseudomonas* sp. RTCS 2 (Fig. 8A) and 1 ± 0.1 mm for *Staphylococcus* sp. RTTS2 (Fig. 8B). This stark contrast highlighted the enhanced antibacterial efficacy of AgNPs, which is attributed to their nanoscale physicochemical properties, allowing more efficient interactions with bacterial cells than larger molecules like sericin. These findings are in consistent with those of the previous works of Wang *et al.*[11] and Masud *et al.*[38]

3.2.4. Minimum inhibitory concentration (MIC). MIC is the minimum concentration of an antimicrobial agent needed to inhibit bacterial growth.[57] In the present study, the MIC values for SS-AgNPs were determined to be 7.8125 μg mL^{-1} for *Pseudomonas* sp. RTCS 2 and 15.625 μg mL^{-1} for *Staphylococcus* sp. RTTS2 (Fig. 9). The MIC for *Pseudomonas* sp. RTCS2 is consistent with values reported for AgNPs synthesized from *Phyllanthus amarus* extract, which ranged from 6.25 to 12.5 ppm against clinical *P. aeruginosa* strains.[58] Elbehiry *et al.*[59] reported

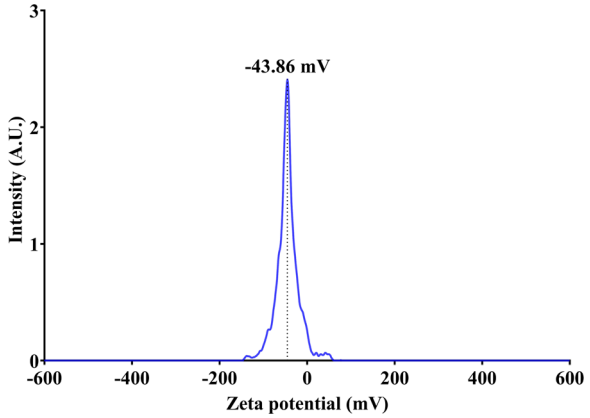

Fig. 5 Zeta potential of bio-molecule-functionalized SS-AgNPs.

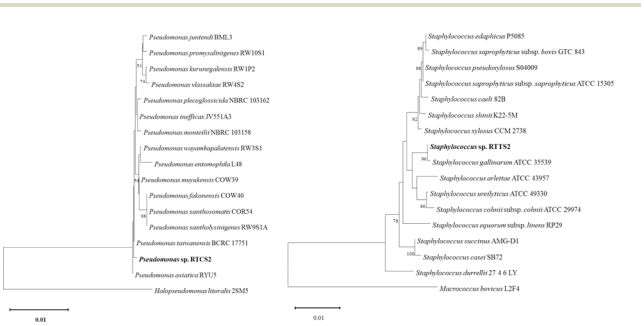

Fig. 6 Neighbor joining phylogenetic tree of the isolated bacteria (*Staphylococcus* sp. RTTS2 and *Pseudomonas* sp. RTCS2) from the control group based on 16s rDNA sequence. Only >50% bootstrap value is shown at the branch node from 1000 replicates.

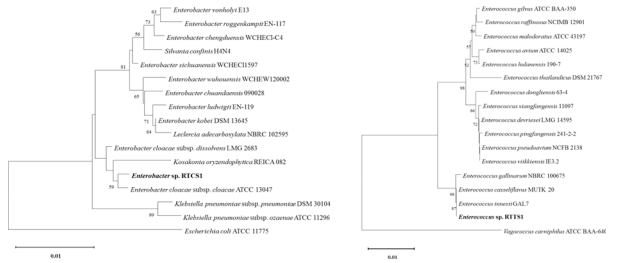

Fig. 7 Neighbor joining phylogenetic tree of the isolated bacteria (*Enterococcus* sp. RTTS1 and *Enterobacter* sp. RTCS1) from the agar-coated group based on 16s rDNA sequence. Only >50% bootstrap value is shown at the branch node from 1000 replicates.

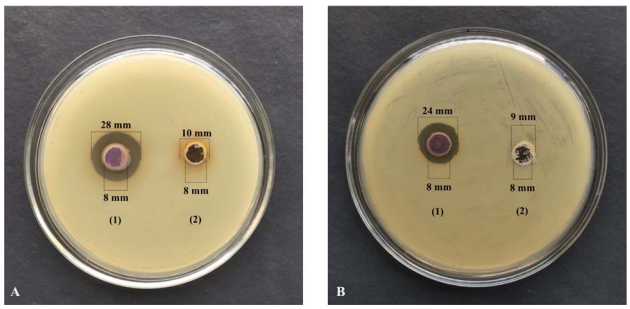

Fig. 8 Measurement of zone of inhibition of (1) SS-AgNPs and (2) 1% (w/v) of SS against (A) *Pseudomonas* sp. RTCS2 and (B) *Staphylococcus* sp. RTTS.

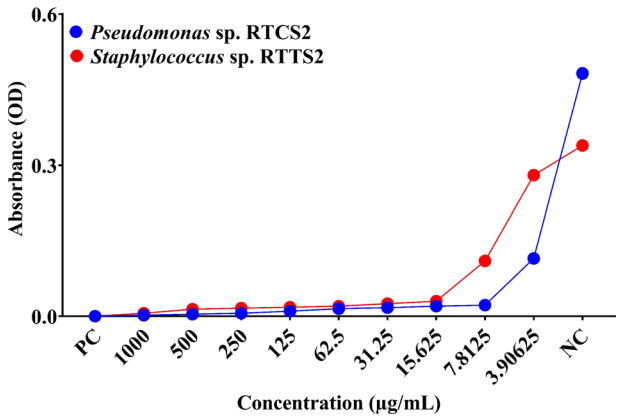

Fig. 9 The MIC (μg mL^{-1}) of the SS-AgNP against the *Pseudomonas* sp. RTCS2 and *Staphylococcus* sp. RTTS2.

that MIC values for AgNPs against *S. aureus* range between 6.25 and 25 μg mL^{-1}. These findings indicate that both bacterial isolates were highly sensitive to SS-AgNPs, and only minimal nanoparticle concentrations were necessary to inhibit the growth of *Staphylococcus* sp. and *Pseudomonas* sp. effectively.

3.3. Biocompatibility of SS-AgNPs

3.3.1. MTT assay. The biocompatibility of SS-AgNPs was evaluated using an MTT assay on HEK293 cells (Fig. 10). Higher cell viability correlates with greater biocompatibility of the

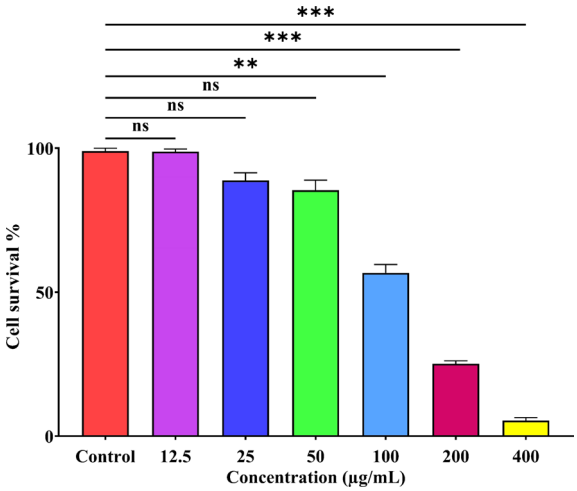

Fig. 10 MTT assay of SS-AgNPs against the HEK293 cell lines. Dunnett's test was employed to compare significant differences between an experimental data set and the control values of that data set; *, **, *** significant at $p < 0.05$ and 0.01, 0.001, respectively.

substance. Results showed that up to 50 μg mL^{-1} of SS-AgNPs did not significantly reduce cell viability compared to the control, indicating good biocompatibility. Similar findings were reported by Some *et al.*,[22] where biosynthesized AgNPs at 50 ppm were also biocompatible with HEK293 cells. Our study suggests that SS-AgNPs selectively target prokaryotic cells, likely due to structural differences in the membranes of prokaryotic and eukaryotic cells. Once internalized through endocytosis, AgNPs dissolve, releasing Ag^{+} ions in the cytosol, which disrupts metabolic processes and the cell cycle.[60]

3.3.2. Hemolysis assay. The hemolysis assay was conducted to evaluate the hemocompatibility of SS-AgNPs. The results indicated that SS-AgNPs at a concentration of 50 μg mL^{-1} caused a hemolysis of 1.153 ± 0.2% (Fig. 11). According to earlier studies, nanoparticles exhibiting less than 5% hemolysis are considered hemocompatible.[61] The controls for the test included a diluted red blood cell (RBC) solution mixed with 0.8 mL of phosphate-buffered saline (PBS) and 0.8 mL of double-distilled water as negative and positive controls, respectively. Additionally, findings by Hajtuch *et al.*[62] support our results, demonstrating that eptifibatide-functionalized

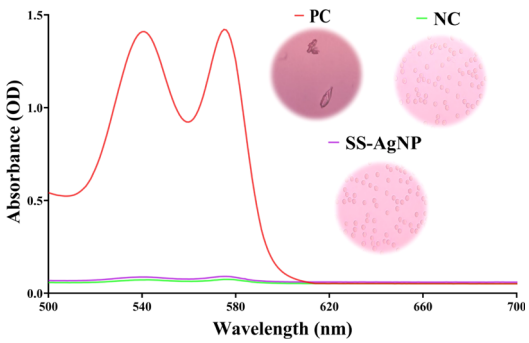

Fig. 11 Hemocompatibility assessment of SS-AgNPs.

silver nanoparticles (AgNPs-EPI) also did not induce significant hemolysis at a concentration of 50 μg mL^{-1}. This corroborates the hemocompatibility of SS-AgNPs. To assess the hemocompatibility of silk sericin-based silver nanoparticles (SS-AgNPs), a hemolysis test was conducted. The results indicated that SS-AgNPs at a concentration of 50 μg mL^{-1} caused a hemolysis of 1.153 ± 0.2%. This corroborates the hemocompatibility of SS-AgNPs.

3.3.3. Toxicity assay on silkworm. The silkworm larvae fed with synthesized SS-AgNPs showed varied responses across measured parameters (Table 3). The shortest larval duration (167.3 h) was recorded at 31.25 μg mL^{-1} (T1), but without significant differences between groups. The highest larval weight (1.34 g) and length (5.267 cm) were observed in the T3 group (125 μg mL^{-1}). No significant changes in silk gland weight were noted. Larval and pupal survivability remained stable across groups, with no notable differences. Cocoon weight (0.840 g) and cocoon shell weight (0.105 g) increased in the T3 group while the cocoon shell percentage slightly increased to 12.58% at 62.5 μg mL^{-1} (T2). Filament length significantly increased to 562.7 meters in T3, while denier decreased to 1.877. Fibroin content increased (84.60% in T2), while sericin content decreased to 15.40% in the same group. Moreover, a significant reduction in denier (1.877) was observed in T3. Results demonstrated that SS-AgNP treatment may improve silkworm traits relevant to silk production. Though larval duration varied slightly, the shorter duration in T1 is beneficial for commercial use. The increased larval weight, length, and filament length in the T3 group, along with stable survivability, suggest no adverse effects on silkworm health. The improved silk fiber quality, evidenced by lower denier and higher fibroin content, supports the use of SS-AgNPs for enhancing silk production. These findings indicated that SS-AgNP-treated leaves could be a valuable addition to sericulture without compromising economic traits.

Previous studies highlighted varied effects of nanoparticles on silkworms, *B. mori*. Li *et al.*[63] found that low concentrations of titanium dioxide nanoparticles (TiO_2 NPs) improved feed efficiency, weight gains, and cocoon mass, while higher concentrations inhibited growth. Similarly, Patil *et al.*[64] reported that AgNPs from mulberry leaf extract using green methods not only enhanced silk protein content but also increased larval weight, cocoon and shell weight.[25] However, AgNPs below 400 μg mL^{-1} were beneficial for growth and cocoon weight, but higher doses led to silkworm mortality.[65] Wu *et al.*[66] observed no significant impact of titanium, iron, and copper nanoparticles on silkworm weight, although they improved silk fibre mechanical properties. Approximately 2000 strains of *B. mori* exhibit diverse traits such as body weight and cocoon weight based on their geographic origin. The interactions between nanoparticles and silkworms, likely driven by the physico-chemical properties and antimicrobial activities of nanoparticles, remain poorly understood.[25,63–66] Further studies are required to investigate the long-term effects of SS-AgNPs on silkworm performance and silk quality.

3.4. Application of SS-AgNPs as food coating material

3.4.1. Determination of weight loss ratio. The study evaluated the efficacy of SS-AgNPs and agar coatings in reducing weight loss in tomatoes during storage. Fig. 12 illustrates the weight loss percentage for tomatoes coated with SS-AgNPs, agar, and uncoated tomatoes over time. As expected, weight loss progressively increased with the duration of storage, with uncoated tomatoes exhibiting the highest weight loss. By the 18th day, the uncoated tomatoes were fully rotten, showing a significant weight loss of 41.74%, which was notably higher than that of SS-AgNPs-coated tomatoes (15.5%) and agar-coated tomatoes (30.19%) (Fig. 12). The superior performance of SS-AgNPs in reducing weight loss compared to agar can be attributed to their antibacterial and barrier properties, which slow down dehydration and spoilage processes.[67,68] On the 12th day of storage, SS-AgNPs-coated tomatoes exhibited the lowest weight loss (10.76%), compared to 16.93% for the agar-coated

Table 3 Effect of feed supplementation with biosynthesized SS-AgNPs on *B. mori*[a]

Parameters	Control	T_1	T_2	T_3
Larval duration (h)	172.0 ± 3.61	167.3 ± 6.66	172.0 ± 6.56	173.0 ± 5.00
Larval weight (g)	1.203 ± 0.05	1.230 ± 0.05	1.247 ± 0.05	1.340 ± 0.03*
Larval length (cm)	4.600 ± 0.20	5.167 ± 0.29	5.200 ± 0.17*	5.267 ± 0.21**
Silk gland weight (g)	0.784 ± 0.01	0.783 ± 0.01	0.844 ± 0.04	0.817 ± 0.04
Larval survivability (%)	95.00 ± 2.00	93.67 ± 1.53	93.33 ± 2.08	93.00 ± 1.00
Pupal survivability (%)	92.33 ± 2.52	89.67 ± 2.08	89.33 ± 2.89	90.00 ± 2.00
Cocoon weight (g)	0.829 ± 0.01	0.817 ± 0.01	0.831 ± 0.01	0.840 ± 0.01
Shell weight (g)	0.100 ± 0.00	0.099 ± 0.00	0.105 ± 0.00	0.105 ± 0.00
Cocoon shell (%)	12.03 ± 0.36	12.16 ± 0.25	12.58 ± 0.54	12.54 ± 0.48
Filament length (m)	483.0 ± 16.09	485.7 ± 11.59	497.7 ± 2.52	562.7 ± 2.52*
Denier (d)	2.257 ± 0.11	2.167 ± 0.12	2.007 ± 0.10	1.877 ± 0.02*
Fibroin content (%)	77.33 ± 3.51	81.00 ± 1.00	84.60 ± 0.4	82.97 ± 0.93
Sericin content (%)	22.67 ± 3.51	19.00 ± 1.00	15.40 ± 0.4	17.03 ± 0.93

[a] Data represent mean ± SD of three replicates; *T*1, *T*2 and *T*3 represent experimental silkworm batches fed with the mulberry leaves spread with synthesized SS-AgNPs at selected concentrations of 31.25 μg mL^{-1}, 62.5 μg mL^{-1} and 125 μg mL^{-1} respectively; Dunnett's test was employed to compare significant differences between an experimental data set and the control values of that data set; *, ** significant at $p < 0.05$ and 0.01, respectively.

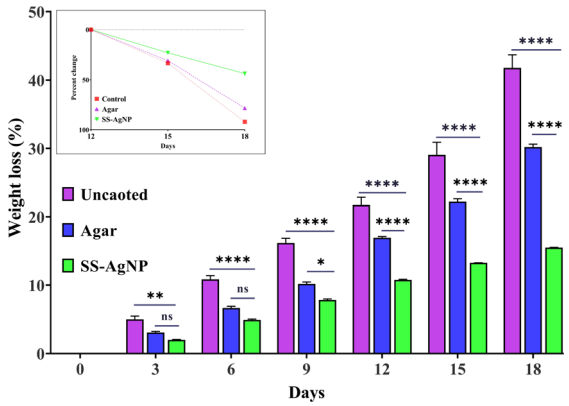

Fig. 12 The effect of SS-AgNPs-based edible coating on weight loss % in tomatoes. In inset the percent loss is calculated from day 12th to day 18th. Dunnett's test was employed to compare significant differences between an experimental data set and the control values of that data set; *, **, **** significant at $p < 0.05$ and 0.01, 0.0001, respectively.

tomatoes. This indicates that SS-AgNPs create a more effective barrier, likely reducing respiration and water loss in the tomatoes.[69] Furthermore, uncoated tomatoes showed a rapid increase in weight loss, reaching up to 92.08% from the 12th to the 18th day. In contrast, SS-AgNPs-coated tomatoes demonstrated a more controlled and gradual weight loss of 44.05% over the same period, as depicted in the inset of Fig. 12. However, further research is needed to detect the exact amount of SS-AgNPs residues present in the fruit/vegetable flesh.

The ability of SS-AgNPs to maintain better moisture content can be linked to their enhanced barrier properties against water vapour and oxygen transmission[70,71] The photographs of tomatoes in the uncoated (control), agar-coated and SS-AgNPs coated across various storage periods is depicted in Fig. 13.

3.4.2. Determination of decaying percentage. The results on determination of decay percentage of tomatoes under different treatment and control groups clearly demonstrated that the decay percentage of tomatoes increased with storage time across the ripening stages. For tomatoes stored at ambient temperature, decay began as early as day 6. At the breaker stage, when the tomato starts to change color from light red to a slightly yellowish red, pink, or dark red, tomatoes showed 23.33% decay by day 6, rising to 40% by day 9, with complete deterioration by day 18 in the control group. In the slightly yellowish red stage, decay accelerated, reaching 26.66% and

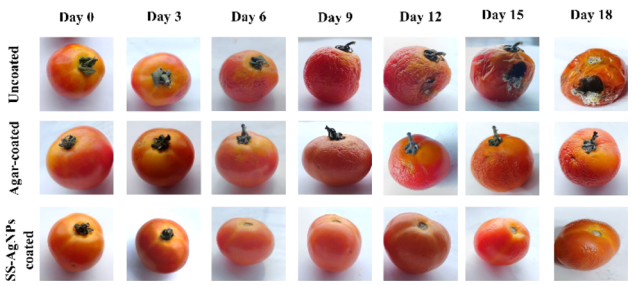

Fig. 13 Photographs of tomatoes in the uncoated, agar-coated and SS-AgNPs coated for 18 days at room temperature.

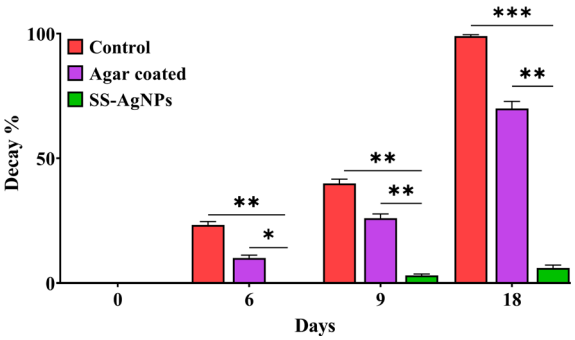

Fig. 14 The effect of SS-AgNPs-based edible coating on decay % in tomatoes. Dunnett's test was employed to compare significant differences between an experimental data set and the control values of that data set; *, ** and *** significant at 0.05, 0.01 and 0.001 respectively.

40% by day 9 both in the control and agar-coated tomatoes. However, a highly significant reduction ($p < 0.01$) in decay percentage was observed in SS-AgNPs-coated tomatoes on day 9 (3%) and day 18 (6%), compared to the control and agar-coated tomatoes (Fig. 14).

The primary factor driving this deterioration is ethylene production, which accelerates fruit ripening corresponding to storage time and temperatures. This aligns with findings by Moneruzzaman *et al.*[72] , who reported that temperatures and humidity are some of the major factors of early decay in fruits. A similar study was conducted earlier to study the decay percentages of postharvest quality of tomatoes under the various storage methods and ripening stages.[34] The schematic diagram presented in Scheme 3 illustrates the protective effect of SS-AgNPs on tomatoes. Uncoated tomatoes are prone to bacterial colonization, leading to decay while, SS-AgNP-coated tomatoes experienced reduced bacterial growth due to the release of silver ions that inhibit bacterial activity. The coating also minimizes weight loss by reducing moisture and gas exchange, ultimately helping to preserve the tomatoes and keep them healthy.

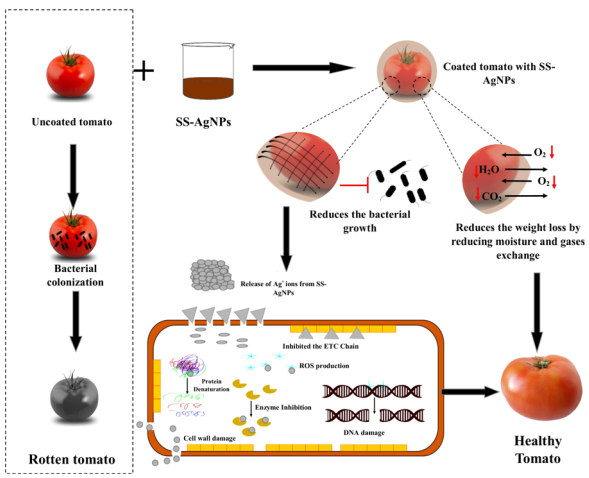

Scheme 3 Schematic diagram of possible protective mechanism of SS-AgNPs on tomatoes.

4. Conclusions

The present study successfully synthesized SS-AgNPs through a simple, eco-friendly method using sericin as both a reducing and stabilizing agent. The comprehensive characterization of the SS-AgNPs confirmed their stability, small size, and high crystallinity, which contributed to their potent antimicrobial activity. The SS-AgNPs demonstrated significant inhibition against common food spoilage bacteria, highlighting their potential in antibacterial applications. Additionally, their use as a food coating material proved effective in reducing weight loss and extending the shelf life of tomatoes, making them a promising solution for food packaging and preservation. Importantly, the biocompatibility assays showed that the SS-AgNPs were non-toxic to human cells and hemocompatible, reinforcing their safety for practical applications in both the biomedical and food industries. This research not only offers a sustainable way to repurpose sericin, a silk industry byproduct, but also opens new avenues for its use in nanotechnology. Future studies could explore the long-term effects of SS-AgNPs in various applications, including larger-scale food packaging systems and advanced biomedical applications, to further realize their full potential. The results from this study pave the way for integrating sericin into commercial products, contributing to a more sustainable and economically viable sericulture industry.

Data availability

The data supporting this article is included in the manuscript.

Conflicts of interest

There are no conflicts to declare.

Acknowledgements

S. S. would like to acknowledge the University Grant Commission, Government of India, for the UGC-JRF fellowship (UGC-JRF; NTA Ref. No. 201610120606). R. M. would like to acknowledge the DST, Govt. of India, for the DST-INSPIRE Fellowship (DST-INSPIRE-SRF; INSPIRE CODE-IF190457). P. D. was provided with an independent PhD Fellowship (UGC-SRF; NTA Ref. No. 201610181190). A. K. M. would like to acknowledge DST-SERB India (EEQ/2021/000058). Authors would also like to acknowledge Mr Pankaj Mandal and Mr Sujoy Sarkar at the Department of Sericulture, Raiganj University for their technical cooperation.

References

1 R. I. Kunz, R. M. C. Brancalhão, L. de, F. C. Ribeiro and M. R. M. Natali, *BioMed Res. Int.*, 2016, **2016**, 8175701.
2 G. Das, H.-S. Shin, E. V. R. Campos, L. F. Fraceto, M. del Pilar Rodriguez-Torres, K. C. F. Mariano, D. R. de Araujo, F. Fernández-Luqueño, R. Grillo and J. K. Patra, *J. Nanobiotechnol.*, 2021, **19**, 30.
3 S.-J. Seo, G. Das, H.-S. Shin and J. K. Patra, *Int. J. Mol. Sci.*, 2023, **24**, 4951.
4 A. S. Silva, E. C. Costa, S. Reis, C. Spencer, R. C. Calhelha, S. P. Miguel, M. P. Ribeiro, L. Barros, J. A. Vaz and P. Coutinho, *Polymers*, 2022, **14**, 4931.
5 D. Hu, T. Li, W. Liang, Y. Wang, M. Feng and J. Sun, *J. Controlled Release*, 2023, **353**, 303–316.
6 P. Chitichotpanya and C. Chitichotpanya, *Coatings*, 2017, **7**, 145.
7 P. Aramwit, S. Damrongsakkul, S. Kanokpanont and T. Srichana, *Biotechnol. Appl. Biochem.*, 2010, **55**, 91–98.
8 M. Sasaki, H. Yamada and N. Kato, *Nutr. Res.*, 2000, **20**, 1505–1511.
9 C. Yang, L. Yao and L. Zhang, *Smart Mater. Med.*, 2023, **4**, 447–459.
10 A. Kumar Dan, B. Aamna, S. De, M. Pereira-Silva, R. Sahu, A. Cláudia Paiva-Santos and S. Parida, *J. Mol. Liq.*, 2022, **368**, 120717.
11 Y. Wang, R. Cai, G. Tao, P. Wang, H. Zuo, P. Zhao, A. Umar and H. He, *Molecules*, 2018, **23**, 1821.
12 H. Muhammad Tahir, F. Saleem, S. Ali, Q. U. Ain, A. Fazal, M. Summer, R. Mushtaq, M. Tariq Zahid, I. Liaqat and G. Murtaza, *J. Basic Microbiol.*, 2020, **60**, 458–467.
13 P. Nie, Y. Zhao and H. Xu, *Ecotoxicol. Environ. Saf.*, 2023, **253**, 114636.
14 Z. Ferdous and A. Nemmar, *Int. J. Mol. Sci.*, 2020, **21**, 2375.
15 M. Carbone, D. T. Donia, G. Sabbatella and R. Antiochia, *J. King Saud Univ. Sci.*, 2016, **28**, 273–279.
16 R. K. Gupta, F. A. E. Gawad, E. A. E. Ali, S. Karunanithi, P. Yugiani and P. P. Srivastav, *Meas. Food*, 2024, **13**, 100131.
17 E. Nanosilver, *State of the Science Literature Review: Everything Nanosilver and More*, US Environmental Protection Agency, Washington, DC, 2010, EPA/600/R-10/084.
18 J. Nam, Y. Hyun, S. Oh, J. Park, H.-J. Jin and H. W. Kwak, *Polym. Test.*, 2021, **97**, 107161.
19 Z. Gün Gök, K. Günay, M. Arslan, M. Yiğitoğlu and İ. Vargel, *Polym. Bull.*, 2020, **77**, 1649–1665.
20 J. Osorio-Echavarría, J. Osorio-Echavarría, C. P. Ossa-Orozco and N. A. Gómez-Vanegas, *Sci. Rep.*, 2021, **11**, 3842.
21 P. Aramwit, N. Bang, J. Ratanavaraporn and S. Ekgasit, *Nanoscale Res. Lett.*, 2014, **9**, 79.
22 S. Some, B. Sarkar, K. Biswas, T. K. Jana, D. Bhattacharjya, P. Dam, R. Mondal, A. Kumar, A. K. Deb and A. Sadat, *RSC Adv.*, 2020, **10**, 22742–22757.
23 B. D. Cullity and R. Smoluchowski, *Phys. Today*, 1957, **10**, 50.
24 R. Heu, S. Shahbazmohamadi, J. Yorston and P. Capeder, *Microsc. Today*, 2019, **27**, 32–36.
25 S. Some, O. Bulut, K. Biswas, A. Kumar, A. Roy, I. K. Sen, A. Mandal, O. L. Franco, İ. A. İnce, K. Neog, S. Das, S. Pradhan, S. Dutta, D. Bhattacharjya, S. Saha, P. K. Das Mohapatra, A. Bhuimali, B. G. Unni, A. Kati, A. K. Mandal, M. D. Yilmaz and I. Ocsoy, *Sci. Rep.*, 2019, **9**, 14839.
26 R. M. Atlas, *Principles of Microbiology*, Wm. C. Brown Publishers, Dubuque, IA, 2nd edn, 1997.
27 J. Marmur, *J. Mol. Biol.*, 1961, **3**, 208–218.

28 D.-P. Mao, Q. Zhou, C.-Y. Chen and Z.-X. Quan, *BMC Microbiol.*, 2012, **12**, 66.
29 R. Mondal, J. Chakraborty, P. Dam, S. Shaw, D. Gangopadhyay, Y. N. Ertas and A. K. Mandal, *ACS Appl. Bio Mater.*, 2024, **7**, 5740–5753.
30 G. Ganga, *An Introduction to Sericulture*, Oxford and IBH Publishing, 2019.
31 S. B. Dandin and V. Kumari, in *Mulberry*, CRC Press, 2021.
32 Y. Feng, J. Lin, L. Niu, P. Pan, X. Liu, L. Huang, Y. Guo and M. Li, *J. Renewable Mater.*, 2023, **11**, 167–184.
33 K. Tarangini, P. Kavi and K. Jagajjanani Rao, *eFood*, 2022, **3**, e36.
34 E. Abiso, N. Satheesh and A. Hailu, *Ann.: Food Sci. Technol.*, 2015, **16**, 127–137.
35 M. Summer, S. Ali, H. M. Tahir, R. Abaidullah, H. Tahir, S. Mumtaz, S. Mumtaz, S. A. Butt and M. Tariq, *Macromol. Chem. Phys.*, 2023, **224**, 2300124.
36 I. Khan, K. Saeed and I. Khan, *Arab. J. Chem.*, 2019, **12**, 908–931.
37 P. Dam, S. Shaw, R. Mondal, J. Chakraborty, T. Bhattacharjee, I. K. Sen, S. Manna, A. Sadat, S. Suin, H. Sarkar, Y. N. Ertas and A. K. Mandal, *RSC Adv.*, 2024, **14**, 26723–26737.
38 Md. A. Al Masud, H. Shaikh, Md. S. Alam, M. M. Karim, M. A. Momin, M. A. Islam and G. M. A. Khan, *J. Genet. Eng. Biotechnol.*, 2021, **19**, 74.
39 S. Mumtaz, S. Ali, A. Pervaiz, M. Z. Qureshi, K. Kanwal and T. Saleem, *Saudi J. Biol. Sci.*, 2023, **30**, 103551.
40 A. Anghileri, R. Lantto, K. Kruus, C. Arosio and G. Freddi, *J. Biotechnol.*, 2007, **127**, 508–519.
41 M. Boulet-Audet, F. Vollrath and C. Holland, *J. Exp. Biol.*, 2015, 128306.
42 P. R. Laity, S. E. Gilks and C. Holland, *Polymer*, 2015, **67**, 28–39.
43 M. Mehdi, H. Qiu, B. Dai, R. F. Qureshi, S. Hussain, M. Yousif, P. Gao and Z. Khatri, *Polymers*, 2021, **13**, 1411.
44 X. Lv, H. Wang, A. Su and Y. Chu, *J. Microbiol. Biotechnol.*, 2018, **28**, 1367–1375.
45 A. J. Kora and J. Arunachalam, *J. Nanomater.*, 2012, **2012**, 869765.
46 L. Liu, R. Cai, Y. Wang, G. Tao, L. Ai, P. Wang, M. Yang, H. Zuo, P. Zhao and H. He, *Int. J. Mol. Sci.*, 2018, **19**, 2875.
47 S. Arokiyaraj, M. Valan Arasu, S. Vincent, Y.-K. Oh, K. H. Kim, K.-C. Choi, S. H. Choi and N. U. Prakash, *Int. J. Nanomed.*, 2014, 379.
48 R. Koley, A. Mondal and N. K. Mondal, *Energy, Ecol. Environ.*, 2023, **8**, 537–555.
49 J. Kanoujia, M. Faizan, P. Parashar, N. Singh and S. A. Saraf, *Food Hydrocolloids Health*, 2021, **1**, 100029.
50 M. Khan, A. U. Khan, I. S. Moon, R. Felimban, R. Alserihi, W. F. Alsanie and M. Alam, *Nanotechnol. Rev.*, 2021, **10**, 1789–1800.
51 M. Riaz, M. Altaf, M. Ayaz, M. A. Sherkheli and A. Islam, *Inorg. Nano-Met. Chem.*, 2021, **51**, 1379–1385.
52 A. H. Labulo, O. A. David and A. D. Terna, *Chem. Pap.*, 2022, **76**, 7313–7325.
53 A. Verma and F. Stellacci, *Small*, 2010, **6**, 12–21.
54 O. Pryshchepa, P. Pomastowski and B. Buszewski, *Adv. Colloid Interface Sci.*, 2020, **284**, 102246.
55 I. Ivanišević, M. Kovačić, M. Zubak, A. Ressler, S. Krivačić, Z. Katančić, I. Gudan Pavlović and P. Kassal, *Nanomaterials*, 2022, **12**, 4252.
56 C. Stan, *General Standard for Fruit Juices and Nectars*, 2005, vol. 247, pp. 1–19, CODEX STAN 247-2005.
57 J. M. Andrews, *J. Antimicrob. Chemother.*, 2001, **48**, 5–16.
58 K. Singh, M. Panghal, S. Kadyan, U. Chaudhary and J. P. Yadav, *J. Nanobiotechnol.*, 2014, **12**, 40.
59 A. Elbehiry, M. Al-Dubaib, E. Marzouk and I. Moussa, *MicrobiologyOpen*, 2019, **8**, e00698.
60 B. Molleman and T. Hiemstra, *Langmuir*, 2015, **31**, 13361–13372.
61 J. Nesa, S. K. Jana, A. Sadat, K. Biswas, A. Kati, O. Kaya, R. Mondal, P. Dam, M. Thakur and A. Kumar, *Sci. Rep.*, 2022, **12**, 15493.
62 J. Hajtuch, E. Iwicka, A. Szczoczarz, D. Flis, E. Megiel, P. Cieciórski, M. W. Radomski, M. J. Santos-Martinez and I. Inkielewicz-Stepniak, *Int. J. Nanomed.*, 2022, **17**, 4383–4400.
63 Y. Li, M. Ni, F. Li, H. Zhang, K. Xu, X. Zhao, J. Tian, J. Hu, B. Wang, W. Shen and B. Li, *Biol. Trace Elem. Res.*, 2016, **169**, 382–386.
64 R. R. Patil, H. R. Naika, S. G. Rayar, N. Balashanmugam, V. Uppar and A. Bhattacharyya, *Part. Sci. Technol.*, 2017, **35**, 291–297.
65 X. Meng, N. Abdlli, N. Wang, P. Lü, Z. Nie, X. Dong, S. Lu and K. Chen, *Biol. Trace Elem. Res.*, 2017, **180**, 327–337.
66 G. Wu, P. Song, D. Zhang, Z. Liu, L. Li, H. Huang, H. Zhao, N. Wang and Y. Zhu, *Int. J. Biol. Macromol.*, 2017, **104**, 533–538.
67 S.-I. Hong, Y. Cho and J.-W. Rhim, *Membranes*, 2021, **11**, 750.
68 J. A. Gudadhe, A. Yadav, A. Gade, P. D. Marcato, N. Durán and M. Rai, *IET Nanobiotechnol.*, 2014, **8**, 190–195.
69 N. Kumar, Neeraj, Pratibha and A. Trajkovska Petkoska, *ACS Food Sci. Technol.*, 2021, **1**, 500–510.
70 S. Liu, L. Li, B. Li, J. Zhu and X. Li, *Carbohydr. Polym.*, 2022, **296**, 119935.
71 S. S. Karkhanis, N. M. Stark, R. C. Sabo and L. M. Matuana, *Composites, Part A*, 2018, **114**, 204–211.
72 K. M. Moneruzzaman, A. Hossain, W. Sani, M. Saifuddin and M. Alenazi, *Aust. J. Crop. Sci.*, 2009, **3**, 113–121.